Carbon Nanotube/Manganese Oxide Ultrathin Film Electrodes for Electrochemical Capacitors

Seung Woo Lee,[†,⊥] Junhyung Kim,[‡,⊥] Shuo Chen,[‡] Paula T. Hammond,[†,*] and Yang Shao-Horn[‡,§,⊥,*]

[†]Department of Chemical Engineering, [‡]Department of Mechanical Engineering, [§]Department of Materials Science and Engineering, and [⊥]Electrochemical Energy Laboratory, Massachusetts Institute of Technology, Cambridge, Massachusetts 02139

ABSTRACT Multiwall carbon nanotube (MWNT)/manganese oxide (MnO_2) nanocomposite ultrathin film electrodes have been created *via* redox deposition of MnO_2 on layer-by-layer (LbL)-assembled MWNT films. We demonstrate that these LbL-assembled MWNT (LbL-MWNT)/MnO_2 thin films consist of a uniform coating of nanosized MnO_2 on the MWNT network structure using SEM and TEM, which is a promising structure for electrochemical capacitor applications. LbL-MWNT/MnO_2 electrodes yield a significantly higher volumetric capacitance of 246 F/cm^3 with good capacity retention up to 1000 mV/s due to rapid transport of electrons and ions within the electrodes. The electrodes are generated with two simple aqueous deposition processes: the layer-by-layer assembly of MWNTs followed by redox deposition of MnO_2 at ambient conditions, thus providing a straightforward approach to the fabrication of high-power and -energy electrochemical capacitors with precise control of electrode thickness at nanometer scales.

KEYWORDS: layer-by-layer self-assembly · carbon nanotube · manganese oxide · nanocomposite electrodes · electrochemical capacitors · energy storage

Electrochemical capacitors (ECs), sometimes called supercapacitors or ultracapacitors, are electrical energy storage devices for various high-power applications such as hybrid electric vehicles and load-leveling.[1,2] Due to the fast charge storage mechanism of double-layer capacitance, which is confined to the interface between the electrode and an electrolyte, ECs have higher power density (~10 kW/kg) but exhibit a lower energy density (~5 Wh/kg) than batteries.[2] However, applications such as hybrid electric vehicles and load-leveling demand significant increases in both energy and power density of electrochemical capacitors to meet their performance and cost requirements.[2,3]

Conventional electrochemical capacitors generated with state-of-the-art electrode materials such as high surface area carbon,[2,4−6] including activated carbon, carbon aerogel, and carbon nanotubes,[7] have stored energy densities measured in specific capacitance on the order of ~150 F/g and ~100 F/cm^3,[4,5,8,9] which linearly scales with electrical double-layer capacitance (EDLC) in ~20 μF/cm$^2_{carbon}$ and electrochemically active surface area. It is very challenging to further increase the specific and volumetric capacitances of such electrodes due to difficulties in controlling pore size, electrochemically active surface area, and surface chemistry. To increase the energy densities of electrochemical capacitors, metal oxides that undergo fast surface redox (pseudocapacitive) reactions are employed. Ruthenium oxide, RuO_2, shows a high specific capacitance of ~720 F/g[10,11] in acidic electrolytes due to its high electrical conductivity and pseudocapacitance with protons; however, it also suffers from high cost. On the other hand, because of its low cost and toxicity, manganese oxides such as MnO_2, which have a long history as positive electrode materials for batteries,[12] have recently attracted attention as promising materials for the enhancement of the energy density of electrochemical capacitors.[13] The theoretical specific capacitance of MnO_2 is ~1370 F/g$_{MnO_2}$ based on a one-electron redox reaction per manganese atom,[14] but this value can be achieved only for ultrathin (on the nanometer scale) films or nanosized particles at the typical power required for electrochemical capacitor applications.[13,14] In addition, activated carbon[15] with surface oxygen showed high capacitance of ~400 F/g and ~200 F/cm^3 at low rates. However, getting sufficient electron access to MnO_2 that has low electrical conductivity (10^{-5}−10^{-6} S/cm)[13] and to surface oxygens on activated carbon (where activation process decreases electrical conductivities and capacitance quickly decreases with increasing current densities[15]) can become rate-limiting for high-power applications. Therefore, maximizing utilization of MnO_2 pseudocapacity and

*Address correspondence to hammond@mit.edu, shaohorn@mit.edu.

Received for review April 4, 2010 and accepted June 04, 2010.

Published online June 16, 2010.
10.1021/nn100681d

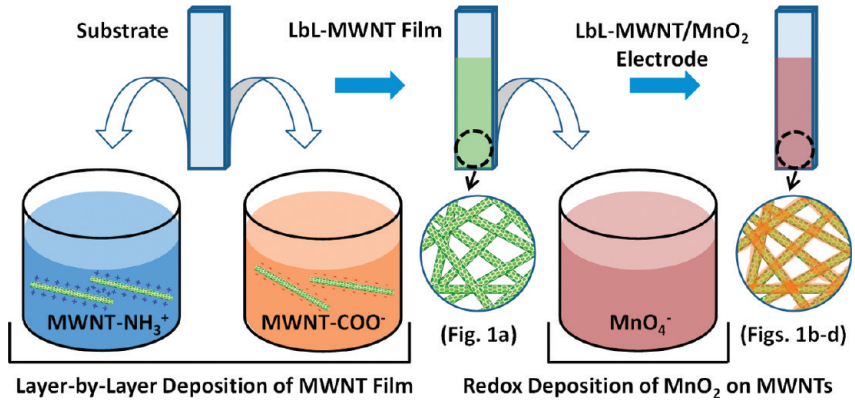

Scheme 1. Layer-by-layer assembly of MWNT (LbL-MWNT) film *via* alternative dipping of substrate into positively charged ($MWNT\text{-}NH_3^+$) and negatively charged ($MWNT\text{-}COO^-$) MWNTs, and prepare LbL-MWNT/MnO_2 electrodes through dipping of the LbL-MWNT film into permanganate ion (MnO_4^-) solution.

designing highly electrically conductive electrode microstructures is critical to realize MnO_2-based electrochemical capacitors.

One promising approach is the incorporation of nanosized MnO_2 into an electrically conductive carbon framework,[2] improving the utilization of MnO_2 and electrical conductivity of the electrode. These carbon matrix/metal oxide nanocomposite electrodes have been demonstrated with various kinds of carbons, including carbon nanotubes,[16−21] carbon nanofoams,[22,23] and activated carbon,[24,25] showing a significant increase in performance. The key issues of carbon matrix/MnO_2 are conformal coatings of nanosized MnO_2 onto a carbon matrix, enabling full utilization of MnO_2, and an interconnected 3D porous network structure that ensures fast electronic and ionic conduction through the electrode. With optimized nanocomposite structures, we can fully utilize the high-energy density of MnO_2 at high-power density for real electrochemical capacitor applications.

Previously, we have created ultrathin multiwall carbon nanotube films using layer-by-layer (LbL) assembly[26] with surface-functionalized multiwall carbon nanotubes (MWNTs).[27] These LbL-assembled MWNT (LbL-MWNT) thin films have interconnected 3D porous network structures and show high capacitance (~130 F/cm^3) in acidic electrolytes.[27] The porous structure of LbL-MWNT films allows further incorporation of electrochemically active nanomaterials that can increase energy density of electrochemical capacitors. In particular, this approach can significantly increase energy density based on volume when nanoscale materials are used to fill the void volume of the carbon matrix. However, generating a homogeneous conformal coating of nanoscale materials within the compact ultrathin MWNT matrix can be challenging. In this study, we incorporate nanoscale MnO_2 films into LbL-MWNT electrodes by electroless deposition using permanganate (MnO_4^-)[28,29] (Scheme 1), and the resulting LbL-MWNT/MnO_2 electrodes show a considerably high volumetric capacitance of ~246 F/cm^3 in neutral electrolytes. The use of MWNTs having high electrical conductivity in the LbL electrodes, instead of single-wall carbon nanotube (SWNTs) that can be metallic or semiconducting,[30] is critical to ensure MnO_2 coating electrochemically active. We show that the structure of the LbL-MWNT/MnO_2 electrodes consists of a nanoscale conformal coating of MnO_2 on interconnected MWNTs in a random network structure using scanning electron microscopy (SEM) and high-resolution scanning transmission electron microscopy (STEM). Cyclic voltammetry measurements reveal that these LbL-MWNT/MnO_2 electrodes have high specific capacitance even at extremely high scan rates (up to 1000 mV/s), which can be attributed to the presence of pseudocapacitive MnO_2 nanoparticles connected to the electrically conductive MWNTs. Finally, we demonstrate the unique advantages of LbL processing, which include the precise control of thickness on the nanometer scale, which enables pinpoint control of electrode capacity with thicknesses in the range of ~100 to ~350 nm.

RESULTS AND DISCUSSION

Ultrathin LbL-MWNT films were created by alternating adsorption of positively charged MWNTs ($MWNT\text{-}NH_3^+$) and negatively charged MWNTs ($MWNT\text{-}COO^-$) on ITO-coated glass substrates. By simply controlling the number of dipping cycles (the number of bilayers), we can precisely assemble pure MWNT films on the substrate with thicknesses in the range from 100 to 350 nm. To increase the mechanical stability and electrical conductivity of the electrodes, LbL-MWNTs were heat treated at 150 °C for 12 h in vacuum[27] before the incorporation of MnO_2. Heat-treated LbL-MWNT films were dipped into a stirred 0.1 M $KMnO_4$/0.1 M K_2SO_4 solution for 10−60 min to incorporate MnO_2 at room temperature. Previous studies[29] have suggested that MnO_4^- ions can be reduced spontaneously to MnO_2 on the surface of MWNTs by oxidizing exterior carbon by the following redox reaction:

$$4MnO_4^- + 3C + H_2O \leftrightarrow 4MnO_2 + CO_3^{2-} + 2HCO_3^- \quad (1)$$

This proposed mechanism is further supported by detection of CO_2 gas as well as formation of CO_3^{2-} and HCO_3^- ions by carrying out this reaction on acetylene black.[28] As this redox reaction is expected to initiate on defect sites of MWNTs,[29] defect sites associated with functionalized groups on LbL-MWNTs can facilitate the redox deposition of MnO_2. Increases in both thickness and mass of the electrodes after incorporation of MnO_2 were observed *via* profilometry and inductively coupled plasma-atomic emission spectroscopy (ICP-AES) analysis: ~10% of thickness (~17% of mass) after 30 min dipping and ~20% of thickness (~36% of mass) after 60 min dipping. Because the LbL assembly process is water-based assembly at ambient conditions, we can consider the spontaneous aqueous deposition of MnO_2 into LbL-MWNT films as a last step of the dipping process, which maintains the continuous nature of the film assembly process.

SEM images (Figure 1) show MnO_2-covered MWNTs created by the spontaneous reduction process on LbL-MWNT films. As-assembled LbL-MWNT films have porous network structure of MWNTs (Figure 1a), where void volume within the porous MWNT matrix allows MnO_4^- ions to diffuse into the films and be reduced to MnO_2 on the surface of MWNTs. From dipping of the LbL-MWNT film into $KMnO_4$ solution for 10 min, we can clearly see a uniform coating of MnO_2 on the MWNT surfaces (Figure 1b), and the thickness of this MnO_2 coating increases as dipping time increases, as indicated by the increasing tube diameters observed in SEM (Figure 1b,c). These SEM top-view images confirm that LbL-MWNT/MnO_2 electrodes have no large agglomerates or precipitation of MnO_2 on the exterior film surface and still maintain a porous network structure after incorporation MnO_2 film into the inner network structure of LbL-MWNT. A cross-section SEM image (Figure 1d) reveals uniform thickness conformal nanocomposite structure of LbL-MWNT/MnO_2 electrode on the substrate without phase segregation of MnO_2 within the electrode. More importantly, cross-sectional elemental mapping of Mn for LbL-MWNT/MnO_2 electrode (Figure 2a) shows uniform distribution of Mn throughout the thickness direction, further confirming uniform introduction of MnO_2 into ultrathin LbL-MWNT electrode. In addition, STEM X-ray elemental mapping of the electrode at a higher magnification (Figure 2b−d) shows a homogeneous distribution of O and Mn on MWNTs, further confirming a homogeneous coating of MnO_2 throughout the LbL-MWNT framework. These conformal coatings of nanoscale MnO_2 on MWNTs suggest a promising nanocomposite structure for energy storage application, where we can fully utilize high capacitance of MnO_2 through electrically conducting MWNT channels.

TEM imaging and selected-area electron diffraction (SAED) analysis were used to determine the crystallinity of MnO_2 and the microstructure of LbL-MWNT/MnO_2 electrodes, as shown in Figure 3. A representative TEM image of an LbL-MWNT electrode in Figure 3a shows a randomly oriented network structure of MWNTs, and the corresponding SAED in the inset reveals graphite characteristic planes of (002), (100), and (110). After 60 min dipping, MnO_2 nanoparticles were found uniformly distributed throughout the MWNT matrix, where MnO_2 nanoparticles on MWNTs are indicated by white arrows in Figure 3c. SAED of the LBL-MWNT/MnO_2 electrode

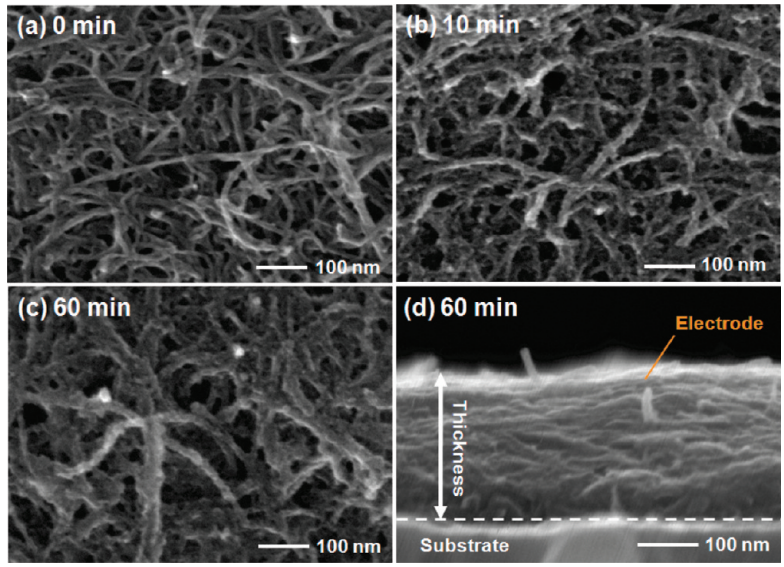

Figure 1. SEM images of (a) pristine LbL-MWNT electrode and (b−d) LbL-MWNT/MnO_2 electrodes prepared by dipping LbL-MWNT electrodes into 0.1 M $KMnO_4$/0.1 M K_2SO_4 solution at a deposition time from 10 to 60 min. (d) Cross-section view of an LbL-MWNT/MnO_2 electrode (10 bilayers, 240 nm, 60 min dipping). White dashed line indicates the interface between the ITO-coated glass substrate and LbL-MWNT/MnO_2 electrode.

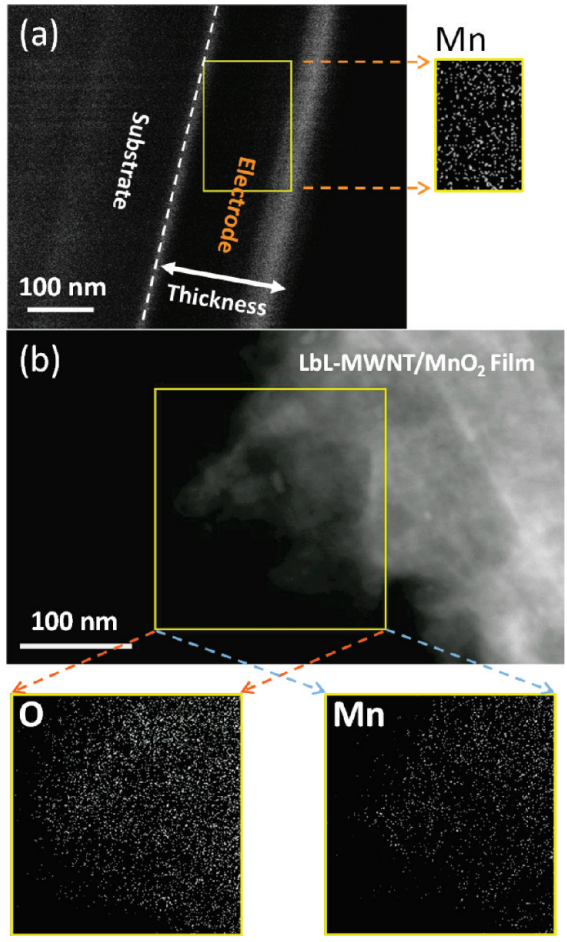

Figure 2. (a) Cross-section SEM image and elemental mapping of Mn for an LbL-MWNT/MnO_2 electrode (10 bilayers, 60 min dipping). White dashed line indicates the interface between the ITO-coated glass substrate and LbL-MWNT/MnO_2 electrode. (b) STEM image with elemental mapping of O and Mn for an LbL-MWNT/MnO_2 electrode slice (10 bilayers, 60 min dipping).

showed only disperse rings of graphite, indicative of the amorphous nature of deposited MnO_2. Previous research has shown that similar redox deposition of MnO_2 on carbon forms an amorphous phase at short time and birnessite MnO_2 at long time (20 h).[23]

X-ray photoelectron spectroscopy (XPS) spectra of the LbL-MWNT/MnO_2 electrodes were used to determine the oxidation state of as-synthesized MnO_2 within the LbL-MWNT film. Mn 2p spectra (Figure 4a) show that the binding energy of Mn $2p_{3/2}$ and Mn $2p_{1/2}$ is centered at 654.1 and 642.4 eV, respectively, which is in agreement with the binding energy of Mn $2p_{3/2}$ and the energy separation (11.8 eV) between $2p_{3/2}$ and $2p_{3/2}$ reported previously.[14,31] Toupin *et al.*[14] show that the separation of peak energies (ΔE_b) between the two peaks of the Mn 3s components can be used as an indicator of Mn oxidation state in manganese oxides, where Mn^{4+} and Mn^{3+} of MnO_2 have a peak separation of ~4.8 and ~5.3 eV, respectively.[14] The as-prepared LbL-MWNT/MnO_2 electrodes after 60 min dipping showed a separation energy of 4.93 eV for the Mn 3s doublet (Figure 4b), which suggest an intermediate oxidation state between Mn^{4+} and Mn^{3+}.

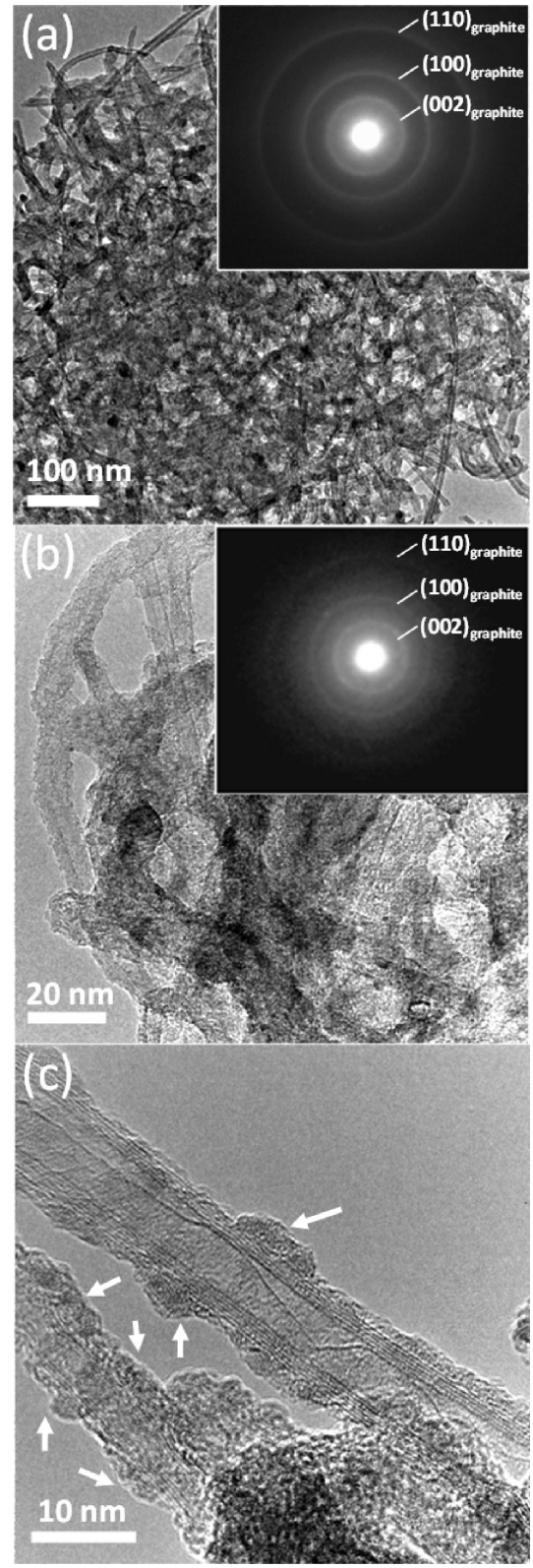

Figure 3. TEM image with selected-area diffraction pattern (SAED) of (a) an LbL-MWNT and (b) an LbL-MWNT/MnO_2 electrode (10 bilayers, 60 min dipping). (c) High-magnification image of an LbL-MWNT/MnO_2 electrode (10 bilayers, 60 min dipping). White arrows indicate nanosize MnO_2 coating on MWNTs.

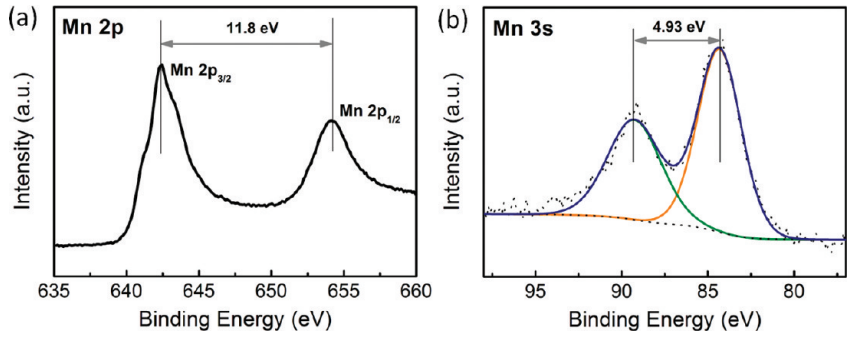

Figure 4. Representative XPS spectra of LbL-MWNT/MnO_2 electrodes. (a) Mn 2p spectra, and (b) Mn 3s spectra.

Figure 5a shows the cyclic voltamogramm (CV) of LbL-MWNT/MnO_2 electrodes in 0.1 M K_2SO_4 at a scan rate of 50 mV/s as a function of dipping time. The potential window for cycling is confined between −0.05 and 0.8 V *versus* SCE to avoid the oxygen evolution reaction at higher potentials and manganese dissolution at lower potentials.[13,24,25] The as-assembled LbL-MWNT electrode (0 min in Figure 5a) shows ~1.8 A/cm^3 based on EDLC of MWNTs. Volumetric currents of the LbL-MWNT/MnO_2 electrodes increase with dipping time due to increasing pseudocapacitive MnO_2, which results in increasing volumetric capacitance with dipping time (Figure 5b). Previous research[16,32] has shown that crystalline

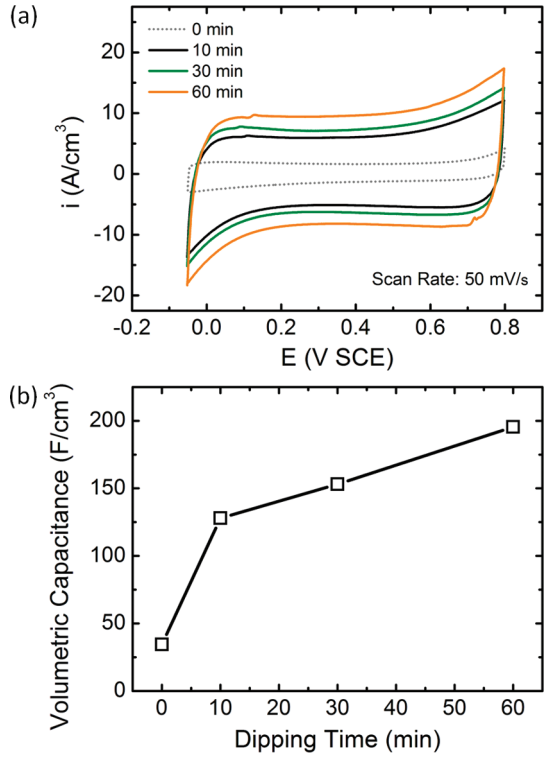

Figure 5. (a) Cyclic voltammograms for LbL-MWNT/MnO_2 films (10 bilayers, 220−240 nm) on ITO-coated glass electrodes in 0.1 K_2SO_4 at room temperature as a function of dipping time. A scan rate of 50 mV/s was used; 0 min indicates a pristine LbL-MWNT electrode. (b) Volumetric capacitance as a function of dipping time. Capacitance was estimated from cyclic voltammograms with a scan rate of 50 mV/s (a).

MnO_2 in K_2SO_4 solution has redox peaks from the intercalation/deintercalation process of the cations. It is interesting that the LbL-MWNT/MnO_2 electrodes have no such redox peaks, which can be related to the amorphous character of MnO_2 films on MWNTs (Figure 3).

We can fully utilize the advantages of the LbL process, enabling precise capacity control of the electrodes by controlling the thickness of LbL-MWNT films. Figure 6a shows a thickness-dependent CV of the MWNT/MnO_2 electrodes in the range from 110 to 350 nm at a scan rate of 50 mV/s. The thicknesses of LbL-MWNT/MnO_2 electrodes still scale with the number of bilayers after 30 min dipping, as shown in Figure 6b, thus suggesting that the coverage of MnO_2 is uniform throughout the thickness of the LbL-MWNT films. Surface charge densities from the integration of CV curves were found to scale linearly with film thickness (Figure 6c) for both the LbL-MWNT films and the LbL-MWNT/MnO_2 electrodes. It should be noted that LbL-MWNT/MnO_2 electrode has a higher slope but the same intercept compared to those of LbL-MWNT, which can be attributed to uniform introduction of MnO_2 throughout the electrode thickness. If MnO_2 deposited only on the surface of LbL-MWNT films, LbL-MWNT/MnO_2 electrode has the same slope but higher intercept compared to those of LbL-MWNT because of the same footprint area of electrodes. Therefore, these results suggest that MnO_2 within the LbL-MWNT electrodes is distributed uniformly and is electrochemically active throughout the entire electrode thickness.

The rate-dependent CVs of LbL-MWNT/MnO_2 electrodes were investigated over a wide range of scan rates from 10 to 1000 mV/s, as shown in Figure 7a. The rate capability of the LbL-MWNT/MnO_2 electrodes is remarkable, and they maintain a rectangular CV shape with only small distortions even at 1000 mV/s, which results in only ~50% loss of capacitance compared to those measured at 10 mV/s (Figure 7b). This is in contrast to previous work, where the rectangular shape of the CV for MnO_2 electrodes[18] was found to distort considerably to a diamond shape as the scan rate increased, and carbon nanotube/carbon microfiber/MnO_2 electrodes[16]

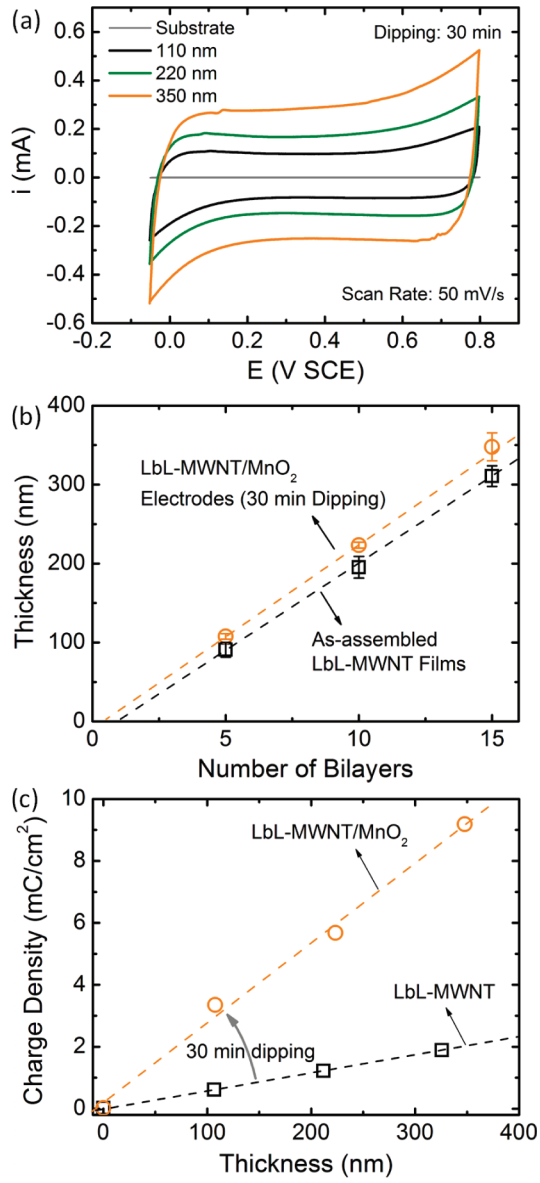

Figure 6. (a) Cyclic voltammograms obtained from LbL-MWNT/MnO_2 electrodes with different thicknesses on ITO-coated glass electrode in 0.1 M K_2SO_4 at room temperature. A scan rate of 50 mV/s was used. (b) Thickness of as-assembled MWNT thin films and LbL-MWNT/MnO_2 electrodes after 30 min dipping as a function of the number of bilayers. The dashed lines are linear fit with standard deviations as error bars. (c) Charge density (measured from cyclic voltammograms and electrode area) *vs* thickness of films from profilometry measurements.

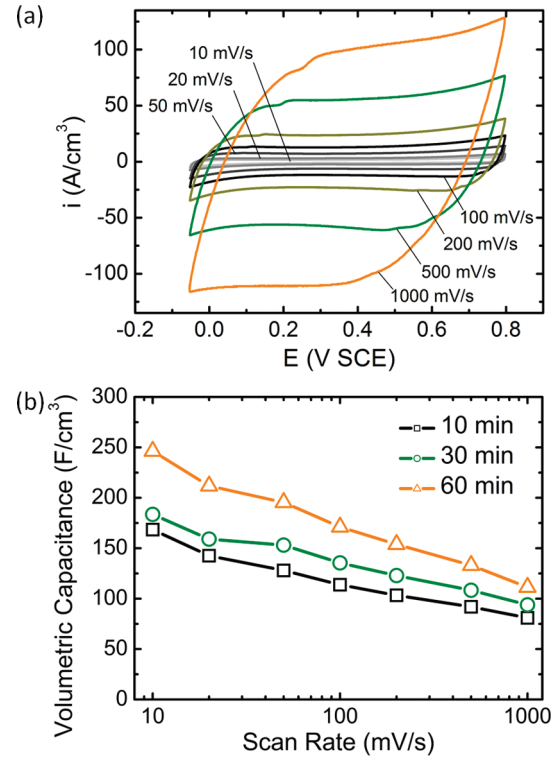

Figure 7. (a) Rate-dependent cyclic voltammograms of LbL-MWNT/MnO_2 electrodes (220 nm, 30 min dipping) at various scan rates (10 to 1000 mV/s). (b) Volumetric capacitance (F/cm^3) obtained from LbL-MWNT/MnO_2 electrodes with dipping time as a function of scan rates (10 to 1000 mV/s).

showed ~50% loss of capacitance from 10 to 200 mV/s. Moreover, LbL-MWNT/MnO_2 electrodes coated for 60 min show a volumetric capacitance of 246 F/cm^3 at a scan rate of 10 mV/s (~1.8 A/cm^3), which is higher than some of the highest reported previously: 132 F/cm^3 for LbL-MWNT electrodes at a scan rate of 50 mV/s (~7 A/cm^3),[27] 156 F/cm^3 for carbon/MnO_2 electrodes[23] at a scan rate of 2 mV/s (~0.4 A/cm^3), and ~150 F/cm^3 for activated carbon activated with oxygen[15] at a current density of ~1 A/cm^3. Furthermore, the high volumetric capacitances of LbL-MWNT/MnO_2 electrodes were obtained at much higher current densities (in A/cm^3 and A/g) than those used in previous studies.[15,17,22,23] The corresponding specific capacitance (*C*) of the LbL-MWNT/MnO_2 electrodes is ~290 F/$g_{LbL\text{-}MWNT/MnO_2}$ while the specific capacitance of MnO_2 (~940 F/g_{MnO_2}) is calculated after subtracting the charge of LbL-MWNT framework (~58 F/g_{MWNT}) according to the following equation

$$C(MnO_2) = \frac{Q(MWNT/MnO_2) - Q(MWNT)}{\Delta V \times m(MnO_2)} \quad (2)$$

where *C* (F/g) is specific capacitance, *Q* is voltammetric charge, ΔV is the width of potential window, and *m* is mass. The specific capacitance of MnO_2 within the LbL-MWNT electrode is significantly higher than that reported previously for redox reduction in carbon nanofoam (~350 F/g)[23] and approaching the thin film MnO_2 and the theoretical value of MnO_2 (~1370 F/g).[14] The high volumetric capacitance and remarkable rate capability of LbL-MWNT/MnO_2 electrodes can be attributed to electrode microstructure, where nanoscale MnO_2 particles are supported on a high-packing density, porous MWNT network with good access to electrons and ions in the electrolyte. In addition, the LbL-MWNT/MnO_2 electrodes show good cycling stability up to

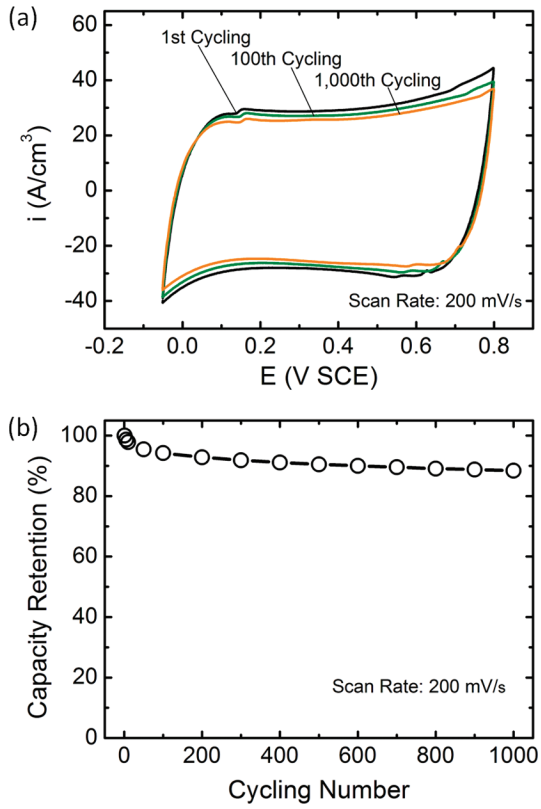

Figure 8. (a) Cyclic voltammograms obtained from LbL-MWNT/MnO_2 electrodes (220 nm, 30 min dipping) with different cycling numbers in 0.1 M K_2SO_4 at room temperature. A scan rate of 200 mV/s was used. (b) Capacity retention from LbL-MWNT/MnO_2 electrodes as a function of cycling number.

1000 cycles, where CVs show very small current reduction (Figure 8a) and capacity (~11.6% decay) during cycling (Figure 8b).

CONCLUSIONS

In summary, we created LbL-MWNT/MnO_2 ultrathin film electrodes *via* an LbL assembly of functionalized MWNTs and continuous redox deposition of MnO_2 onto MWNTs. The porous MWNT network generated *via* alternating LbL assembly creates fast electronic and ionic conducting channels in the presence of electrolyte, and the conformal coating of MnO_2 on MWNTs provides high capacitance, which shows that these systems can provide a platform to design high-performance electrodes for electrochemical capacitor applications. The ability to generate high electrode capacitances and precise control of thickness and capacity from simple dipping processes at ambient conditions suggests a promising approach to the creation of ultrathin electrodes in a controlled manner. We believe that these high-capacitance LbL-MWNT/MnO_2 film electrodes and the general approach to the fabrication of nanostructured electrodes can be applied to design novel electrode materials for EC and battery and sensor applications. In addition, versatile adaptability of the LbL technique on various kinds of substrates such as silicon, glass, and flexible substrates propose binder-free MWNT/MnO_2 electrodes as promising electrodes for application of MEMS flexible electronics.[33]

METHODS

Layer-by-Layer Assembly of MWNT Thin Films. MWNTs were purchased from NANOLAB (95% purity, outer diameter 15 ± 5 nm, length 1−5 μm). Positively charged MWNTs (MWNT-NH_3^+) and negatively charged MWNTs (MWNT-COO^-) were prepared using surface functionalization processes described in previous research.[27] The LbL-MWNT films were fabricated with a modified Carl Zeiss DS50 programmable slide stainer on indium−tin oxide (ITO)-coated glass slides (Delta Technologies). ITO-coated glass slides were first dipped into a MWNT-NH_3^+ solution for 30 min and washed in three baths of Milli-Q water for 2, 1, 1 min each to remove weakly adsorbed MWNTs. Then, the substrates were dipped into a MWNT-COO^- solution for 30 min and three baths of Milli-Q water for 2, 1, 1 min each. This cycle makes one bilayer of MWNT-NH_3^+/MWNT-COO^-, and the cycle was repeated to reach the desired thickness of MWNT thin films. In this study, we control the thickness of LbL-MWNT films from 110 to 350 nm. Detailed procedure and property of LbL-MWNT films can be found in previous research.[27]

Incorporation of MnO_2 into LbL-MWNT Films. Previous studies have shown that spontaneous redox deposition of MnO_2 on carbon materials is pH-dependent.[19,22] Reduction of permanganate ion (MnO_4^-) to MnO_2 on the carbon in acid can result in large agglomerated particles of MnO_2.[16,22] On the other hand, thin films of MnO_2 can be obtained on the surface of carbon in neutral pH, which show higher gravimetric capacitance compared to those of MnO_2 formed in acid.[22,23] In this study, we dipped the LbL-MWNT films into 0.1 M K_2SO_4 (Sigma-Aldrich) + 0.1 M $KMnO_4$ (Sigma-Aldrich) solution from 10 to 60 min to incorporate MnO_2 in neutral condition. To facilitate MnO_4^- diffusion into the LbL-MWNT, films and solutions were stirred vigorously with magnetic stirrer.

Characterization. The thickness of electrodes was determined by averaging the thickness at least four different positions on each electrode using a Tencor P-10 profilometer. The volume of electrode was estimated by multiplying the geometric area of the electrode and measuring average thickness. Inductively coupled plasma-atomic emission spectroscopy (ICP-AES) analysis was used to analyze the weight loading of MnO_2 on the MWNTs using a Horiba-Activa instrument; the measurements were made on emission peaks at 293.306 for Mn. The LbL-MWNT/MnO_2 film sample was dissolved in concentrated aqua regia and then diluted. The diluted solution was filtrated for analysis. Calibration curves were made from dissolved standards with concentrations from 0 to 25 ppm in the same acid matrix as the unknown. Microstructure of the LbL-MWNT/MnO_2 electrode was investigated using a scanning electron microscope (JEOL 6320 SEM) operating at 5.0 kV. For X-ray energy-dispersive spectroscopy (EDS) with SEM, the accelerating voltage is set at 15.0 kV. The acquisition time is 354 s. Inner structure of the LbL-MWNT/MnO_2 electrode was examined using a transmission electron microscope (JEOL 2010F) for medium- and high-resolution imaging, as well as the selected-area electron diffraction (SAED) of the electrode samples. Scanning transmission electron microscopy mode is applied for EDS mapping. The acquisition time is 279 s. Oxygen K_{a1} (0.525 keV), carbon K_{a1} (0.285 keV), and manganese K_{a1} (5.899 keV) lines are used to generate the elemental maps of oxygen, carbon, and manganese, respectively. The surface chemistry of the LbL-MWNT/MnO_2 electrode was investigated using a Kratos AXIS Ultra Imaging X-ray photoelectron spectrometer (XPS). Mn 3s and 2p spectra were calibrated with

the C 1s photoemission peak for sp^2-hybridized carbons centered at 284.5 eV. Electrochemical test of the LbL-MWNT/MnO_2 electrode was measured at a three-electrode cell, using a saturated calomel electrode (SCE) (Analytical Sensor, Inc.) and Pt wire as the reference and counter electrodes, respectively. LbL-MWNT/MnO_2 electrodes were used as the working electrode in 0.1 M K_2SO_4 solution. Cyclic voltammetry was measured in the potential range between −0.05 and 0.8 V *versus* SCE at room temperature at various scan rates from 10 to 1000 mV/s using a bipotentiostat (PINE instrument).

Acknowledgment. This work was supported by the MRSEC Program of the National Science Foundation under the Award No. DMR 08-19762. S.W.L. acknowledges a Samsung Scholarship from the Samsung Foundation of Culture.

REFERENCES AND NOTES

1. Miller, J. R.; Simon, P. Materials Science—Electrochemical Capacitors for Energy Management. *Science* **2008**, *321*, 651–652.
2. Simon, P.; Gogotsi, Y. Materials for Electrochemical Capacitors. *Nat. Mater.* **2008**, *7*, 845–854.
3. Miller, J. R.; Burke, A. Electrochemical Capacitors: Challenges and Opportunities for Real-World Applications. *Electrochem. Soc. Interface* **2008**, *17*, 53–57.
4. Frackowiak, E.; Beguin, F. Carbon Materials for the Electrochemical Storage of Energy in Capacitors. *Carbon* **2001**, *39*, 937–950.
5. Simon, P.; Burke, A. Nanostructured Carbons: Double-Layer Capacitance and More. *Electrochem. Soc. Interface* **2008**, *17*, 38–43.
6. Pandolfo, A. G.; Hollenkamp, A. F. Carbon Properties and Their Role in Supercapacitors. *J. Power Sources* **2006**, *157*, 11–27.
7. Futaba, D. N.; Hata, K.; Yamada, T.; Hiraoka, T.; Hayamizu, Y.; Kakudate, Y.; Tanaike, O.; Hatori, H.; Yumura, M.; Iijima, S. Shape-Engineerable and Highly Densely Packed Single-Walled Carbon Nanotubes and Their Application as Super-capacitor Electrodes. *Nat. Mater.* **2006**, *5*, 987–994.
8. Emmenegger, C.; Mauron, P.; Sudan, P.; Wenger, P.; Hermann, V.; Gallay, R.; Zuttel, A. Investigation of Electrochemical Double-Layer (ECDL) Capacitors Electrodes Based on Carbon Nanotubes and Activated Carbon Materials. *J. Power Sources* **2003**, *124*, 321–329.
9. Kim, Y. J.; Abe, Y.; Yanaglura, T.; Park, K. C.; Shimizu, M.; Iwazaki, T.; Nakagawa, S.; Endo, M.; Dresselhaus, M. S. Easy Preparation of Nitrogen-Enriched Carbon Materials from Peptides of Silk Fibroins and Their Use To Produce a High Volumetric Energy Density in Supercapacitors. *Carbon* **2007**, *45*, 2116–2125.
10. Zheng, J. P.; Cygan, P. J.; Jow, T. R. Hydrous Ruthenium Oxide as an Electrode Material for Electrochemical Capacitors. *J. Electrochem. Soc.* **1995**, *142*, 2699–2703.
11. Zheng, J. P.; Jow, T. R. A New Charge Storage Mechanism for Electrochemical Capacitors. *J. Electrochem. Soc.* **1995**, *142*, L6–L8.
12. Thackeray, M. M. Manganese Oxides for Lithium Batteries. *Prog. Solid State Chem.* **1997**, *25*, 1–71.
13. Bélanger, D.; Brousse, T.; Long, J. W. Manganese Oxides: Battery Materials Make the Leap to Electrochemical Capacitors. *Electrochem. Soc. Interface* **2008**, *17*, 49–52.
14. Toupin, M.; Brousse, T.; Belanger, D. Charge Storage Mechanism of MnO_2 Electrode Used in Aqueous Electrochemical Capacitor. *Chem. Mater.* **2004**, *16*, 3184–3190.
15. Alonso, A.; Ruiz, V.; Blanco, C.; Santamaria, R.; Granda, M.; Menedez, R.; de Jager, S. G. E. Activated Carbon Produced from Sasol-Lurgi Gasifier Pitch and Its Application as Electrodes in Supercapacitors. *Carbon* **2006**, *44*, 441–446.
16. Bordjiba, T.; Belanger, D. Direct Redox Deposition of Manganese Oxide on Multiscaled Carbon Nanotube/Microfiber Carbon Electrode for Electrochemical Capacitor. *J. Electrochem. Soc.* **2009**, *156*, A378–A384.
17. Ma, S. B.; Nam, K. W.; Yoon, W. S.; Yang, X. Q.; Ahn, K. Y.; Oh, K. H.; Kim, K. B. Electrochemical Properties of Manganese Oxide Coated onto Carbon Nanotubes for Energy-Storage Applications. *J. Power Sources* **2008**, *178*, 483–489.
18. Xie, X. F.; Gao, L. Characterization of a Manganese Dioxide/Carbon Nanotube Composite Fabricated Using an *In Situ* Coating Method. *Carbon* **2007**, *45*, 2365–2373.
19. Ma, S. B.; Ahn, K. Y.; Lee, E. S.; Oh, K. H.; Kim, K. B. Synthesis and Characterization of Manganese Dioxide Spontaneously Coated on Carbon Nanotubes. *Carbon* **2007**, *45*, 375–382.
20. Fan, Z. J.; Qie, Z. W.; Wei, T.; Yan, J.; Wang, S. S. Preparation and Characteristics of Nanostructured MnO_2/MWCNTs Using Microwave Irradiation Method. *Mater. Lett.* **2008**, *62*, 3345–3348.
21. Chou, S. L.; Wang, J. Z.; Chew, S. Y.; Liu, H. K.; Dou, S. X. Electrodeposition of MnO_2 Nanowires on Carbon Nanotube Paper as Free-Standing, Flexible Electrode for Supercapacitors. *Electrochem. Commun.* **2008**, *10*, 1724–1727.
22. Fischer, A. E.; Pettigrew, K. A.; Rolison, D. R.; Stroud, R. M.; Long, J. W. Incorporation of Homogeneous, Nanoscale MnO_2 within Ultraporous Carbon Structures *via* Self-Limiting Electroless Deposition: Implications for Electrochemical Capacitors. *Nano Lett.* **2007**, *7*, 281–286.
23. Fischer, A. E.; Saunders, M. P.; Pettigrew, K. A.; Rolison, D. R.; Long, J. W. Electroless Deposition of Nanoscale MnO_2 on Ultraporous Carbon Nanoarchitectures: Correlation of Evolving Pore-Solid Structure and Electrochemical Performance. *J. Electrochem. Soc.* **2008**, *155*, A246–A252.
24. Brousse, T.; Toupin, M.; Belanger, D. A Hybrid Activated Carbon-Manganese Dioxide Capacitor Using a Mild Aqueous Electrolyte. *J. Electrochem. Soc.* **2004**, *151*, A614–A622.
25. Brousse, T.; Taberna, P. L.; Crosnier, O.; Dugas, R.; Guillemet, P.; Scudeller, Y.; Zhou, Y.; Favier, F.; Belanger, D.; Simon, P. Long-Term Cycling Behavior of Asymmetric Activated Carbon/MnO_2 Aqueous Electrochemical Supercapacitor. *J. Power Sources* **2007**, *173*, 633–641.
26. Decher, G. Fuzzy Nanoassemblies: Toward Layered Polymeric Multicomposites. *Science* **1997**, *277*, 1232–1237.
27. Lee, S. W.; Kim, B. S.; Chen, S.; Shao-Horn, Y.; Hammond, P. T. Layer-by-Layer Assembly of All Carbon Nanotube Ultrathin Films for Electrochemical Applications. *J. Am. Chem. Soc.* **2009**, *131*, 671–679.
28. Huang, X. K.; Yue, H. J.; Attia, A.; Yang, Y. Preparation and Properties of Manganese Oxide/Carbon Composites by Reduction of Potassium Permanganate with Acetylene Black. *J. Electrochem. Soc.* **2007**, *154*, A26–A33.
29. Jin, X.; Zhou, W.; Zhang, S.; Chen, G. Z. Nanoscale Microelectrochemical Cells on Carbon Nanotubes. *Small* **2007**, *3*, 1513–1517.
30. Ajayan, P. M. Nanotubes from Carbon. *Chem. Rev.* **1999**, *99*, 1787–1799.
31. Reddy, A. L. M.; Shaijumon, M. M.; Gowda, S. R.; Ajayan, P. M. Coaxial MnO_2/Carbon Nanotube Array Electrodes for High-Performance Lithium Batteries. *Nano Lett.* **2009**, *9*, 1002–1006.
32. Brousse, T.; Toupin, M.; Dugas, R.; Athouel, L.; Crosnier, O.; Belanger, D. Crystalline MnO_2 as Possible Alternatives to Amorphous Compounds in Electrochemical Supercapacitors. *J. Electrochem. Soc.* **2006**, *153*, A2171–A2180.
33. Gates, B. D. Flexible Electronics. *Science* **2009**, *323*, 1566–1567.